

AD A 042546

(Handwritten marks)

DNA 4144F

A DYNAMIC CRATER EJECTA MODEL

Science Applications, Inc
8400 Westpark Drive
McLean, Virginia 22101

30 October 1976

Final Report for Period 1 October 1975—30 September 1976

CONTRACT No. DNA 001-76-C-0023

APPROVED FOR PUBLIC RELEASE;
DISTRIBUTION UNLIMITED.

DDC
AUG 5 1977
C

THIS WORK SPONSORED BY THE DEFENSE NUCLEAR AGENCY
UNDER RDT&E RMSS CODE B344076464 Y99QAXSA00177 H2590D.

DDC FILE COPY

Prepared for
Director
DEFENSE NUCLEAR AGENCY
Washington, D. C. 20305

< -

Destroy this report when it is no longer
needed. Do not return to sender.



UNCLASSIFIED

SECURITY CLASSIFICATION OF THIS PAGE (When Data Entered)

19 REPORT DOCUMENTATION PAGE		READ INSTRUCTIONS BEFORE COMPLETING FORM
1. REPORT NUMBER DNA 4144F	2. GOVT ACCESSION NO.	3. RECIPIENT'S CATALOG NUMBER
4. TITLE (and Subtitle) A DYNAMIC CRATER EJECTA MODEL	5. TYPE OF REPORT & PERIOD COVERED Final Report 1 Oct 75 - 30 Sep 76	6. PERFORMING ORG. REPORT NUMBER SAI-76-654-WA
7. AUTHOR(s) William R. Seebaugh	8. CONTRACT OR GRANT NUMBER(s) DNA 001-76-C-0023	10. PROGRAM ELEMENT PROJECT, TASK AREA & WORK UNIT NUMBERS NWED Subtask Y99QAXSA001-77
9. PERFORMING ORGANIZATION NAME AND ADDRESS Science Applications, Inc. 8400 Westpark Drive McLean, Virginia 22101	11. CONTROLLING OFFICE NAME AND ADDRESS Director Defense Nuclear Agency Washington, D.C. 20305	12. REPORT DATE 30 Oct 76
14. MONITORING AGENCY NAME & ADDRESS (if different from Controlling Office)	13. NUMBER OF PAGES 46 (124 Sp.)	15. SECURITY CLASS (of this report) UNCLASSIFIED
16. DISTRIBUTION STATEMENT (of this Report) Approved for public release; distribution unlimited.		15a. DECLASSIFICATION/DOWNGRADING SCHEDULE
17. DISTRIBUTION STATEMENT (of the abstract entered in Block 20, if different from Report)		
18. SUPPLEMENTARY NOTES This work sponsored by the Defense Nuclear Agency under RDT&E RMSS Code B344076464 Y99QAXSA00177 H2590D.		
19. KEY WORDS (Continue on reverse side if necessary and identify by block number) Crater Ejecta Nuclear Crater High Explosive Crater Debris Hazard		
20. ABSTRACT (Continue on reverse side if necessary and identify by block number) A dynamic model for the high explosive and nuclear crater ejecta environments is presented, together with selected results for a 1 MT surface burst on hard rock. The model provides both the ground deposition and airborne ejecta cloud environments. The effects of explosive type, yield and geology are taken into account in the model. The deposition results are obtained in the form of the cumulative mass and number of fragments impacting the ground plane per unit area, the ejecta depth,		

DDC
APPROVED FOR
AUG 5 1977
RESOLVED
C

DD FORM 1473 1 JAN 73

EDITION OF 1 NOV 65 IS OBSOLETE

UNCLASSIFIED

SECURITY CLASSIFICATION OF THIS PAGE (When Data Entered)

UNCLASSIFIED

SECURITY CLASSIFICATION OF THIS PAGE(When Data Entered)

20. ABSTRACT (Continued)

the fragment size class (minimum and maximum fragment diameters) and the minimum and maximum values of the impact time, velocity, angle, momentum and kinetic energy as functions of range from the burst point. The ejecta cloud environment is given in the form of mass and number densities as functions of spatial position and time.

UNCLASSIFIED

SECURITY CLASSIFICATION OF THIS PAGE(When Data Entered)

PREFACE

This topical report was prepared by Science Applications, Inc. (SAI) in compliance with the requirements of Defense Nuclear Agency Contract DNA001-76-C-0023. The program was sponsored by the Strategic Structures Division of the Shock Physics Directorate of DNA and was performed during the period 01 October 1975 through 30 September 1976. The technical representative of the sponsor was Capt. Jerry R. Stockton.

The program at SAI was performed under the direction of Dr. William R. Seebaugh. He was assisted in the computer analyses by Mr. Elwood E. Zimmerman and Ms. Susan J. Rose.

ACCESSION for	
NTIS	White Section <input checked="" type="checkbox"/>
DDC	Buff Section <input type="checkbox"/>
UNANNOUNCED	<input type="checkbox"/>
JUSTIFICATION	_____
BY	
DISTRIBUTION/AVAILABILITY NOTES	
Di.	_____
_____	_____

TABLE OF CONTENTS

<u>Section</u>		<u>Page</u>
	PREFACE.....	1
1	INTRODUCTION.....	5
2	GENERAL DESCRIPTION OF EJECTA MODEL.....	8
3	THE EJECTA SOURCE.....	11
4	EJECTA TRAJECTORIES.....	22
5	RESULTS AND DISCUSSION.....	27
6	CONCLUDING REMARKS.....	37
	REFERENCES.....	38
	NOMENCLATURE.....	39

LIST OF FIGURES

<u>Figure</u>		<u>Page</u>
1	Ejecta Problem Definition.....	7
2	Ejecta Environment Analysis.....	9
3	Zones of Origin of Crater Ejecta.....	12
4	Cumulative Ejecta Mass from Crater Calculations..	14
5	Correlation of Ejecta Velocity and Fragment Diameter.....	20
6	Fragment Drag Coefficients.....	26
7	Ejecta Depth for 1 MT Surface Burst.....	28
8	Ejecta Area Number Density for 1 MT Surface Burst.....	29
9	Ejecta Fragment Size Class for 1 MT Surface Burst.....	31
10	Ejecta Impact Time for 1 MT Surface Burst.....	32
11	Ejecta Impact Velocity for 1 MT Surface Burst....	33
12	Ejecta Impact Angle for 1 MT Surface Burst.....	34
13	Ejecta Cloud Boundaries for 1 MT Surface Burst...	36

Section 1

INTRODUCTION

The crater ejecta environment for high explosive (HE) and nuclear bursts has been under investigation by Science Applications, Inc. (SAI) for several years. Earlier work on the dynamic crater ejecta model, supported by the Defense Nuclear Agency (DNA), was conducted under Contracts DNA001-73-C-0088, DNA001-74-C-0102 and DNA001-75-C-0102 during the period 20 November 1972 through 30 October 1975. The basic ejecta model was developed during this period. The present effort, which was performed under Contract DNA001-76-C-0023, was concerned with updating the model to incorporate the results of the most recent theoretical calculations and experimental investigations. The period of performance of this contract was 01 October 1975 through 30 September 1976. This report describes the current ejecta model and thus provides a summary of the entire four-year effort.

The ejecta mass represents a substantial fraction of the total mass excavated during the formation of an explosive crater. This mass has been determined for experimental craters by measuring the thicknesses of the post-event ejecta blankets. A number of empirical models for the thickness of the ejecta blanket have been developed; see, for example, Post (Reference 1) and McGetchin et al. (Reference 2). These models are based upon measurements obtained primarily from a large number of HE and nuclear craters. Limited data are also available for the Arizona Meteor Crater and estimates of the ejecta thickness at the crater rim have been made for several lunar craters.

An alternative method of obtaining estimates of the ejecta blanket thickness considers the entire history of the crater formation and ejecta deposition. In this approach, which is the subject of this report, the crater formation and ejecta throwout processes are modeled, the trajectories of representative ejecta fragments are calculated and the ejecta blanket thickness is obtained by summing the contributions

of the fragments impacting the surface. The procedure also provides a description of the airborne ejecta cloud prior to deposition of the ejecta fragments on the surface. The problem is delineated schematically in Figure 1. The left side of the sketch illustrates the positions of the representative fragments a few seconds after the burst. These fragments impact the surface within about a minute of the burst, forming the ejecta blanket as shown on the right side of the sketch. The inner region of the ejecta blanket is characterized by a continuous distribution of material that completely covers the original ground surface. At larger ranges, there is insufficient ejecta mass to cover the surface and the distribution is discontinuous. The ejecta mass is defined as the amount of crater material that crosses the original ground surface and impacts beyond the apparent crater radius (R_a in Figure 1); this definition excludes both fallback and upthrust. The crater lip radius is denoted by R_{a1} .

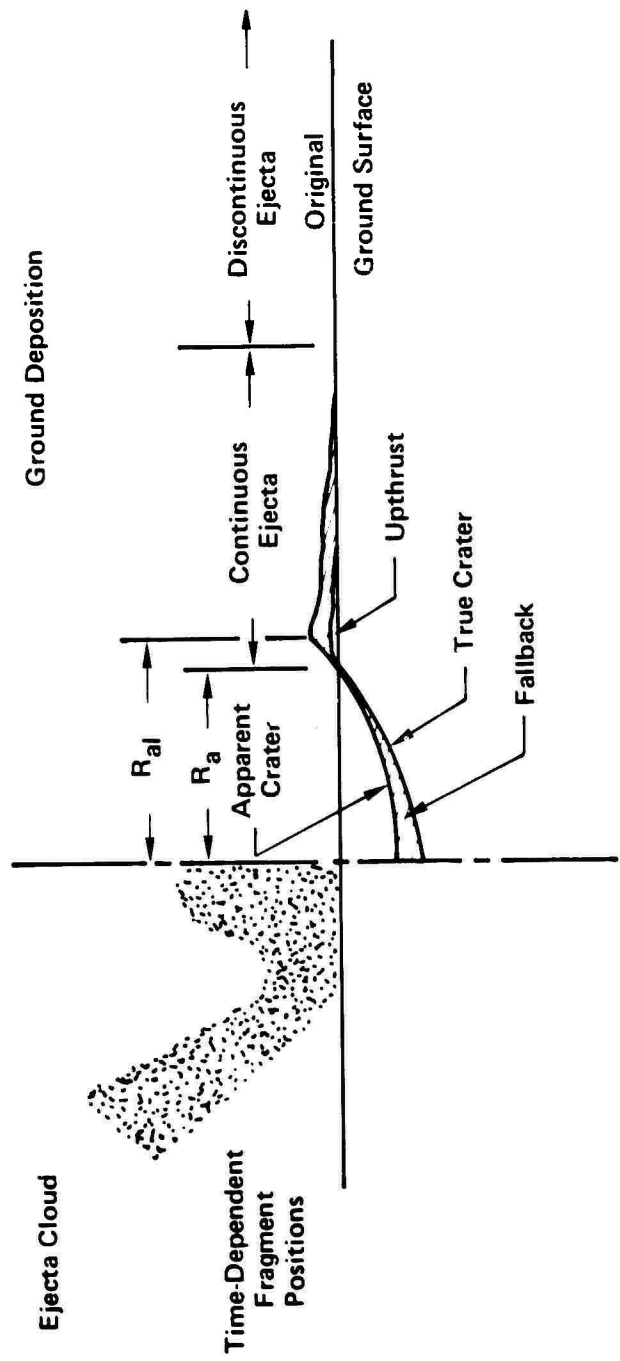


Figure 1. Ejecta Problem Definition

Section 2

GENERAL DESCRIPTION OF EJECTA MODEL

The ejecta model is based upon recent crater calculations, selected low-yield ejecta data (primarily from HE events) and current models of the buoyant fireball and the associated wind field. The model is illustrated in flow chart form in Figure 2. The inputs to the model are:

- (1) Theoretical velocity distribution for continuous hydrodynamic material emerging from the crater
- (2) Empirical models for ejecta mass, fragment size distribution and maximum fragment size
- (3) Experimental observations of fragment velocity for high explosive (HE) shots
- (4) Vortex flow model (VORDUM^a) for the fireball and winds which affect ejecta fragment trajectories
- (5) Compressible flow aerodynamic drag model.

Items (1) through (3) above define the crater source. Ejecta fragments produced by this source are transported through the flowfield defined by the VORDUM program [Item (4) above] using the aerodynamic drag model for ejected crater material [Item (5) above]. The source model and the trajectory calculation form the complete ejecta model as shown in Figure 2. The method of analysis is applicable to the modeling of both the ground deposition of crater ejecta and the airborne ejecta cloud. The deposition results are obtained in the form of the cumulative mass and number of fragments impacting the ground plane per unit area, the ejecta depth, the fragment size class (minimum and maximum fragment diameters) and the minimum and maximum values of the impact time,

^aVORDUM is an acronym for a vortex dust model which was developed to describe the fluid and particulate motion associated with the rise of a buoyant fireball through the earth's atmosphere.

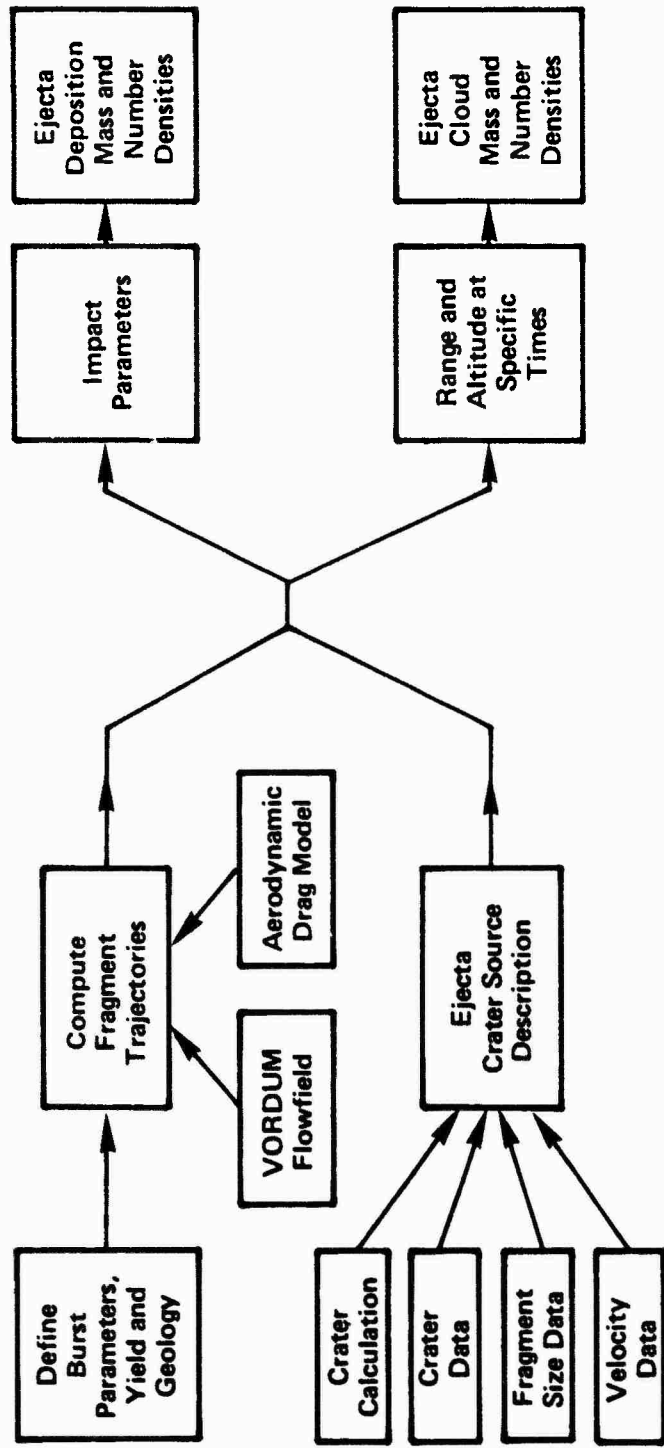


Figure 2. Ejecta Environment Analysis

velocity, angle, momentum and kinetic energy as functions of range from the burst point. The ejecta cloud environment is produced simultaneously. During the VORDUM trajectory calculations (Figure 2), trajectory parameters in the form of range and altitude versus time are recorded for each representative fragment. This information is combined with the crater source description to give airborne ejecta fragment mass and number densities.

Section 3

THE EJECTA SOURCE

The most important assumptions of the ejecta model are related to the ejecta source. The source description must include the mass ejection rate, the ejection velocity (speed and angle) and the fragment size distribution as functions of radius and time. Empirical correlations have been derived for the total ejecta mass (Reference 3) and for the relative origins of ejecta fragments within the crater (Davis and Carnes, Reference 4). The latter correlation is shown in Figure 3 for event MINERAL ROCK, a 100-ton TNT shot on granite. As shown, the ejecta missiles originate from the upper portion of the crater away from the center of the charge. Very little ejecta comes from the region near the axis. Although cratering studies have produced correlations such as those shown in Figure 3, attempts to construct an ejecta source model completely from experimental data have been unsuccessful. Data do not exist on the rate of ejection of material from the crater. The in-flight photography of ejecta fragments may be analyzed to give representative fragment ejection velocities, but such analyses do not relate mass to velocity. It is, therefore, necessary to incorporate results of theoretical calculations into the ejecta source model to complete the source description.

A number of two-dimensional hydrodynamic calculations using advanced elastic-plastic material models have been performed recently. The methods have not been generally successful in predicting the final crater dimensions. It appears that the poor agreement for the final crater volume is a result of failure to properly predict the late-time motion, which occurs at low velocities. The mass of ejecta leaving the crater with higher velocities is not as dependent on the material model as the low-velocity ejecta, and consistent results have been obtained for the high-velocity material by assuming that the ejecta motion is driven by the amount of energy coupled to the ground (defined

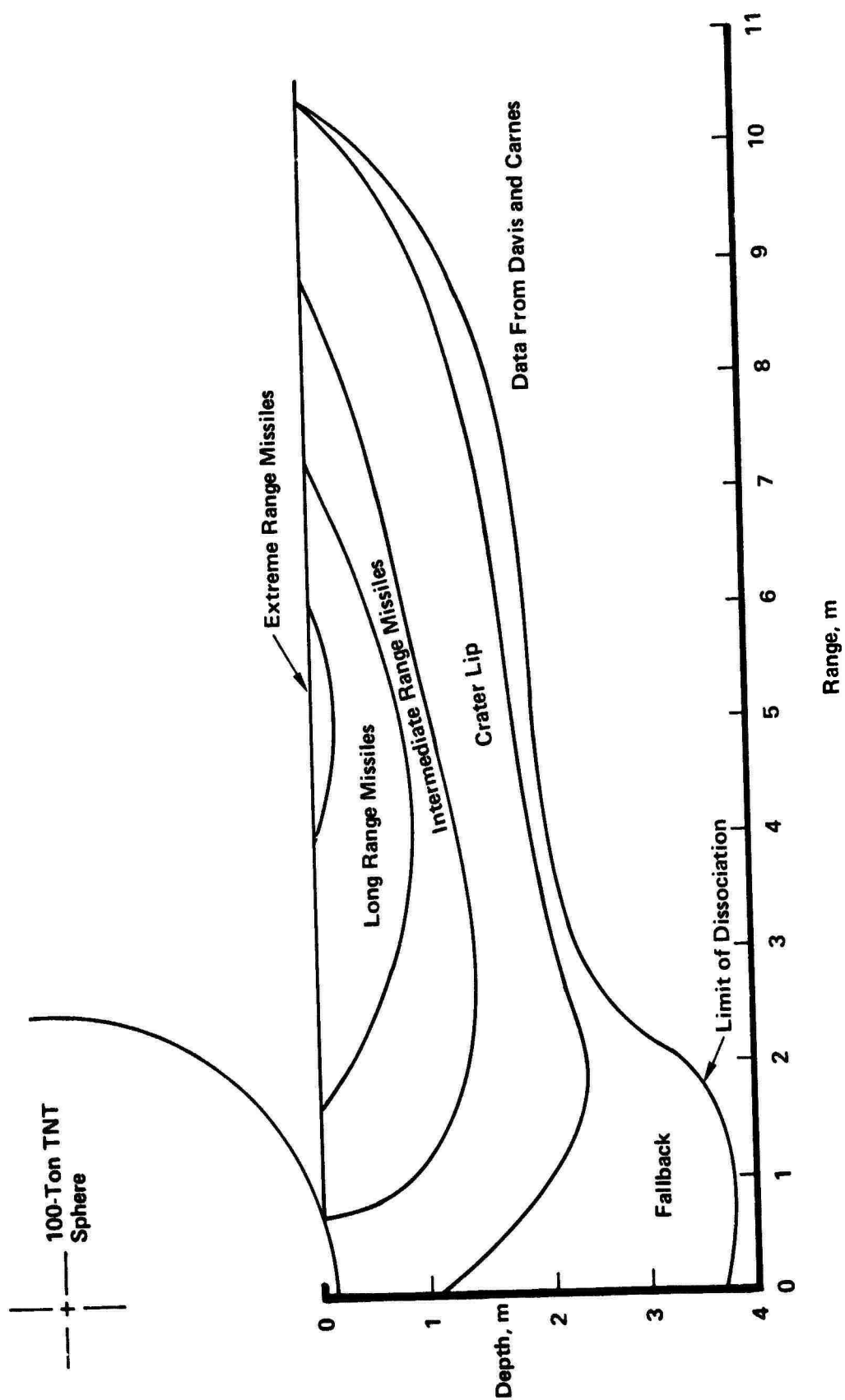


Figure 3. Zones of Origin of Crater Ejecta

as the total energy below the ground surface at 1 μ sec after burst). The results of an analysis of the properties of the crater material crossing the original ground surface for a number of calculations are presented in Figure 4 in the form of average vertical velocity (defined as the ratio of the momentum flux to the mass flux) versus the cumulative ejecta mass with greater average vertical velocity. Curve 1 represents the average relationship for high strength materials (wet tuff and granite), whereas Curve 2 is the average for two calculations of the nuclear event JOHNIE BOY (0.5 kt yield at a depth of burst of 0.6 m in alluvium). These curves suggest the source relationship given by the dashed line in Figure 4 as an upper velocity bound for a nuclear surface burst. The equation of this line may be represented by the function

$$\frac{\partial M}{\partial V} = M_e \frac{V_{\min, z}}{\sin \theta} V^{-2} \quad (1)$$

where $\partial M/\partial V$ is the ratio of the differential ejecta mass δM associated with differential ejection velocity δV , M_e is the ejecta mass, θ is the ejection angle relative to the horizontal and V is the ejection velocity. This function is normalized to give the empirically determined ejecta mass (see below) at a minimum value of the vertical component of the ejection velocity $V_{\min, z}$ of 6.4 m/sec. The minimum velocity considered is then

$$V_{\min} = \frac{(V_{\min, z})}{\sin \theta} = \frac{6.4 \text{ m/sec}}{\sin \theta} \quad (2)$$

The total ejecta mass is determined from correlations of experimental cratering data. Layson (Reference 3) has quoted the relationship

$$M_a = 2.4 W^{0.9} \quad (3)$$

for the apparent crater mass (M_a , megatons) for megaton-range surface bursts on rock, where W is the explosive yield in megatons. Experimental

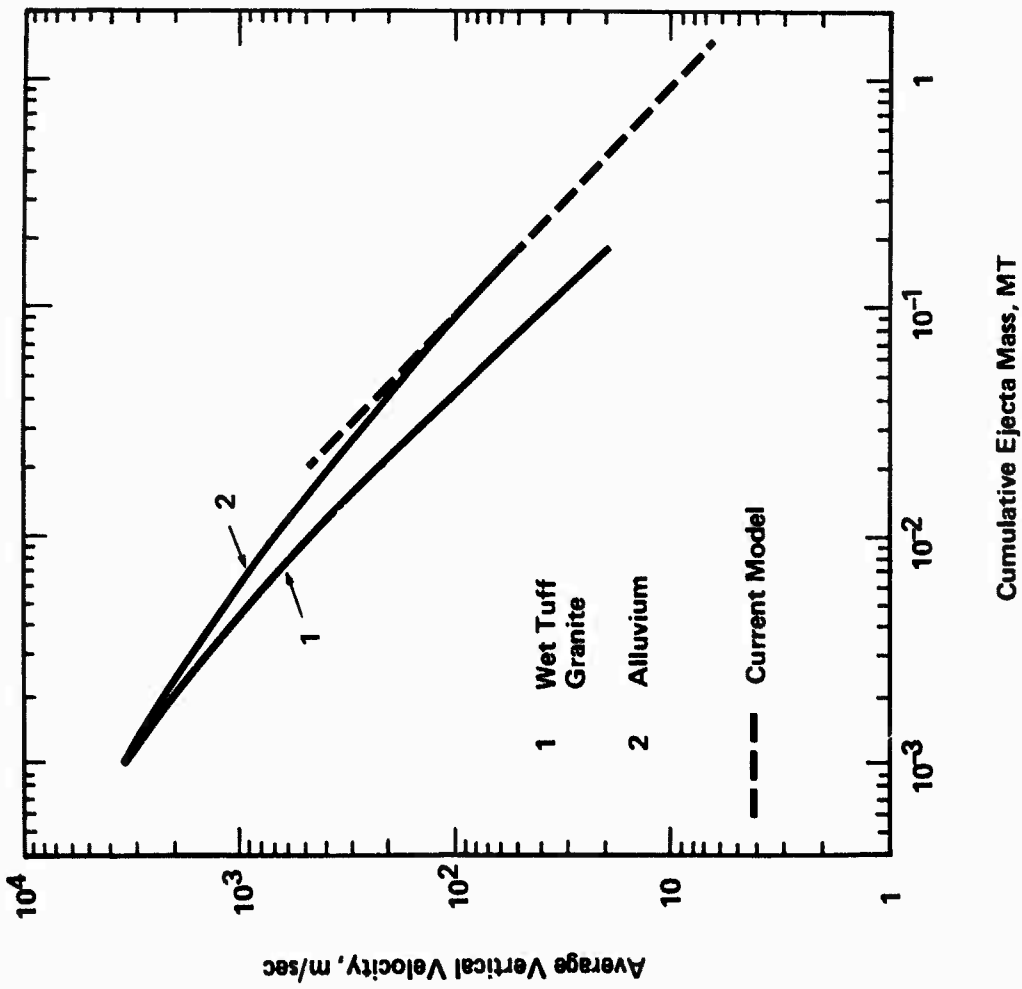


Figure 4. Cumulative Ejecta Mass From Crater Calculations

data (Reference 3) also suggest that the ejecta mass (in megatons) is given by

$$M_e = 0.6 M_a \quad (4)$$

or, combining Equations (3) and (4),

$$M_e = 1.44 W^{0.9} \quad (5)$$

The ejecta mass M_e includes all excavated material crossing the original ground surface, a large part of which emerges from the crater at relatively low velocities and comes to rest on the crater lip (Figure 1). Material with initial vertical velocity below 6.4 m/sec is not included in the ejecta mass M_e .

The apparent crater mass given by Equation (3) corresponds to a cratering efficiency of $0.84 \text{ m}^3/\text{ton}$; this value is in agreement with the mean cratering efficiency given by Post (Reference 1) for hard rock. Limer (Reference 5) examined the geology and height-of-burst dependence of the cratering efficiency and derived the following relationship for apparent crater mass as a function of yield and scaled height of burst (SHOB):

$$M_a = a_1 \rho W K_g K_s \exp(-a_2 \text{ SHOB}) \quad (6)$$

where ρ is the in situ density of the cratering medium (kg/m^3), K_g and K_s are geology and source correction terms and a_1 and a_2 are given by

Source	a_1 (m^3/kg)	a_2 ($\text{kt}^{1/3}/\text{m}$)	SHOB Range ($\text{m}/\text{kt}^{1/3}$)
Nuclear (LYTW and HYTW)	4.8×10^{-3}	1.007	-1.56 to 1.1
	2.06×10^{-2}	0.069	-19.5 to -1.56
HE	4.8×10^{-3}	0.325	-1.79 to 5.18
	2.06×10^{-2}	0.069	-19.5 to -1.79

The cratering medium density and the geology correction term were determined by classifying HE data by generic geologies:

<u>Generic Geology</u>	<u>$\rho(\text{kg/m}^3)$</u>	<u>K_g</u>
Hard Rock	2600	0.5 ± 0.2
Dry Sand-Sandstone	1500	0.58 ± 0.2
Alluvium	1600	1.00 ± 0.23
Clay-Shale	1760	1.89 ± 0.89
Saturated Soil	2100	4.41 ± 0.64

The source correction term distinguishes HE, low yield-to-weight (LYTW) nuclear and high yield-to-weight (HYTW) nuclear sources:

$$\text{HE: } K_s = \begin{cases} 5.71 & (-1.79 \text{ m/kt}^{1/3} < \text{SHOB} < 5.18 \text{ m/kt}^{1/3}) \\ 2.1 & (-19.5 \text{ m/kt}^{1/3} < \text{SHOB} < -1.79 \text{ m/kt}^{1/3}) \end{cases}$$

LYTW

$$\text{Nuclear: } K_s = 1$$

$$\text{HYTW Nuclear: } K_s = \begin{cases} 0.25 & (-0.3 \text{ m/kt}^{1/3} < \text{SHOB} < 1.1 \text{ m/kt}^{1/3}) \\ 0.25 - 0.18(1+3.3 \text{ SHOB}) & (-1.56 \text{ m/kt}^{1/3} < \text{SHOB} < -0.3 \text{ m/kt}^{1/3}) \\ 1 & (\text{SHOB} < -1.56 \text{ m/kt}^{1/3}) \end{cases}$$

Equation (4) is applied to determine the ejecta mass.

Equation (6) gives a cratering efficiency of $0.55 \text{ m}^3/\text{ton}$ for hard rock at $\text{SHOB} = 0$. This is about 35 percent below the aforementioned value quoted by Layson (Reference 3) and Post (Reference 1) and is at the lower end of the scatter band given by Post. Both Liner (Reference 5) and Post (Reference 1) scaled the apparent crater mass linearly with yield, whereas Layson (Reference 3) scaled mass with yield to the 0.9 power. The effects of these differences are within the scatter of the data base from which the various correlations were derived. The

approach developed by Liner [Equation (6)] has been incorporated into the current ejecta model. For the case discussed in Section 5, a cratering efficiency of $0.84 \text{ m}^3/\text{ton}$ [Equation (3)] was used for a 1 MT surface burst over hard rock.

The distribution of the crater mass over the range of possible ejecta fragment sizes is an important ingredient of the ejecta source model. Studies of cratering in rock media such as basalt and granite (Reference 3) indicate that the size distribution has the form

$$\frac{\partial M}{\partial a} = \frac{0.5 M_e}{\sqrt{a_m}} a^{-0.5}, \quad (7)$$

where $\partial M/\partial a$ is the ratio of the differential mass δM associated with the differential fragment diameter δa , over a range of fragment diameter from about 10^{-4} to 1 m. The term a_m is the diameter of the largest ejecta fragment. Gault, et al. (Reference 6) compiled data for explosive and impact cratering events and observed that the correlation for the mass of the largest fragment

$$m_m = 6.6 \times 10^5 M_e^{0.8} \quad (8)$$

was a reasonable representation of the data for a variation of 14 orders of magnitude of M_e . The constant of proportionality gives the maximum fragment mass m_m in kg when M_e is expressed in megatons. Assuming spherical fragments the maximum fragment diameter $a_m(m)$ is give by

$$a_m = \left(\frac{6m_m}{\pi\rho} \right)^{1/3} \quad (9)$$

The in situ density is used in the current model. The size distribution given by Equation (7), with the upper limit given by a_m , is assumed to apply to all cratering media (hard rock, sandstone and so forth) except those clearly defined with alluvial basins or sands with water table levels below the apparent crater depth.

The size distribution for incohesive soils (alluvium and dry sand) is more accurately described by the relationship derived for Nevada Test Site alluvium (Reference 3)

$$\frac{\partial M}{\partial a} = \frac{M_e}{a} \quad (10)$$

The maximum ejecta fragment diameter for such incohesive soils is likely to be more closely associated with the maximum in situ diameter than with the ejecta mass [Equation (8)]. For these situations, the in situ maximum diameter is employed as the upper limit to the distribution given by Equation (10).

There is currently no experimentally based method for selecting size distributions between the limits represented by Equations (8) and (10). Fortunately, the ejecta environment is not extremely sensitive to this parameter. The effects of using the in situ maximum diameter in place of the correlation of Equation (8) [for alluvium and dry sand] increase as the difference between the respective maximum diameters increases. This is a result of the influence of air drag. Further research is required to more accurately define these effects for incohesive cratering media.

The crater mass-velocity relationships derived from the cratering calculations and the experimentally derived fragment size distributions cannot be truly coupled because the process of comminution of the crater material has not been described either theoretically or experimentally. The approach taken in the current ejecta model is to distribute the ejecta mass over the velocity-size spectrum using the aforementioned relationships, and to exclude combinations of velocity and size that appear unreasonable based upon an analysis of additional experimental data.

The basis for a limiting velocity-size relationship is provided by the results of an extensive in-flight ejecta analysis using photography of HE events (Reference 7). The analysis gives the sizes and ejection conditions for a large number of large ejecta fragments. The results for event MIDDLE GUST III, a 100-ton surface tangent TNT shot on a layered (clay over shale) medium, are presented in Figure 5^a. The fragment diameters were obtained by assuming spherical fragments. The data are bounded by two limits:

$$V_{\max} = 566 W^{1/6} \quad (11)$$

and

$$V_m = C V_{\max} \frac{a_m}{a} \quad (12)$$

where velocities are in m/sec. The material ejected at the highest hydrodynamic velocities near the burst (Figure 4) must either be vaporized or pulverized by the shocks measured in hundreds of kilobars. It is not reasonable to associate these high velocities with fragments of significant size. The absolute maximum velocity, Equation (11), performs the required limiting function, with the value of the constant determined from the data of Figure 5. The 1/6-power dependence of velocity on yield was suggested by Sauer and Cooper (Reference 8) and observed experimentally by Wisotski (Reference 7). Qualitative observations of results of field surveys and aerial photography for HE and nuclear events indicate that the largest ejecta fragments do not reach the largest ranges from the burst. The use of a size-dependent maximum velocity, Equation (12), produces the observed results. The form of this limit was also obtained from the data of Figure 5.

^aA small number of fragments (9 out of a total of 151) which required large corrections to obtain the true azimuthal planes of the trajectories were eliminated from the sample. See Reference 7 for an explanation of the correction procedure.

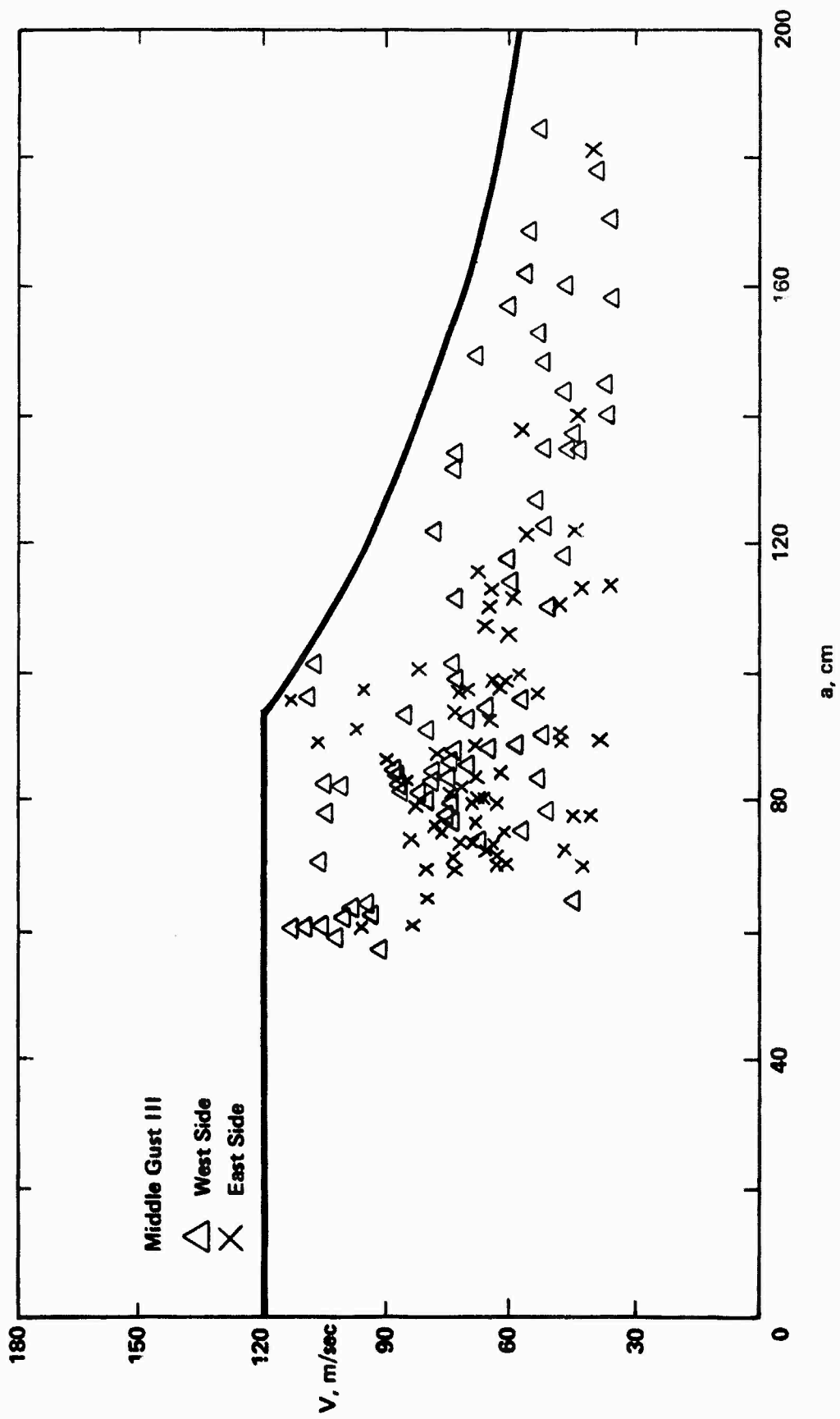


Figure 5. Correlation of Ejecta Velocity and Fragment Diameter

The parameter C is a function of the explosive type (HE or nuclear) and the depth of burst. Tentative values for this parameter are 0.5 for surface tangent HE (for example, event MIDDLE GUST III), 0.3 for half-buried HE and 0.1 for megaton-range nuclear surface bursts. Equation (12) is required only for cohesive media; the limit provided by Equation (11) is sufficient to bound the fragment velocities for incohesive media for which the maximum fragment diameter equals the in situ value. Note that the size-dependent velocity limit shown in Figure 5 was calculated using the experimentally determined ejecta mass in Equation (8).

The relationships given in Equations (1) through (12) define the overall characteristics of the ejecta source. In order to complete the source model, the points of origin of the ejecta fragments within the crater must be specified. The experimental ejecta origin description illustrated in Figure 3 is modeled effectively by a crater model developed by Rosenblatt and Eggum (Reference 9). This model simulates the time phased development of the crater as described by the same hydrodynamic cratering calculations used to determine the mass-velocity relationships shown in Figure 4. The ejection velocity and mass flux across the original ground surface are specified as functions of time (consistent with the dashed line in Figure 4). For cohesive media, each increment of mass is partitioned into a range of fragment sizes according to Equation (7), consistent with the limits specified by Equations (11) and (12). Equations (10) and (11) perform the same functions for incohesive soils. The result is a matrix of representative ejecta fragments, with each fragment characterized by its ejection velocity (speed and angle), diameter, ejection time, location within the developing crater and the ejecta mass that it represents. This matrix provides the initial conditions for the ejecta trajectory calculations.

Section 4

EJECTA TRAJECTORIES

The primary effects of the explosion are to form the crater, to generate a hot low density region near the burst point and to create strong afterwinds which perturb the ejecta trajectories. It is of interest to know more of the motion through the very early fireball environment, but it is beyond the state of the art to describe the details of the interaction of the ejected earth material and the developing early fireball. The most reliable way to circumvent this difficulty is to make good calculations of the trajectories after pressure equilibration while adjusting the source description to obtain good agreement with the available HE and nuclear test data. This is the approach that has been followed in the development of the current ejecta model.

A relatively simple hydrodynamic model, VORDUM, has been developed to describe the air and dust/debris motion inside and around a rising cloud. In this model, the early-time dust cloud is a buoyant vortex whose flowfields entrain dust particles and distribute them through space according to their initial position, mass, and aerodynamic drag characteristics. Within the fireball radius, the aerodynamic drag is calculated for air at one-tenth ambient density. Trajectories of larger ejecta fragments are perturbed by the wind field. The boundary condition at the ground — no normal velocity component at the ground surface — is satisfied by imposing an image vortex system that moves away from the ground in the negative field. As the cloud rises, it expands adiabatically and also mixes with the ambient air. The rates at which the cloud rises and expands were obtained from test data and hydrodynamic cloud calculations.

A number of trace fragment trajectories is computed for each ejecta environment description desired. Cylindrical symmetry is assumed at all times during the calculation. The VORDUM output consists of range and altitude coordinates describing each trace fragment trajectory. Each trace fragment corresponds to many actual fragments; the ejecta mass corresponding to each representative fragment is obtained from Equations (1) and (7) for cohesive cratering media, and from Equations (1) and (10) for incohesive soils.

Perhaps the most important assumption in the trajectory calculation relates to the drag coefficient. Previous studies have used values measured for smooth spheres, but as explained below, this assumption is not appropriate for ejecta fragments and the present model employs a different drag model. The standard drag curves for flow over a smooth sphere are given in Hoerner (Reference 10). The range of Reynolds numbers^a of interest in the ejecta trajectory calculations is from about 10^3 to 10^6 . For incompressible flow, the drag coefficient C_D remains nominally constant in the region of laminar boundary-layer flow from $Re = 10^3$ to about 3×10^5 . In this regime, a substantial portion of the total drag is the pressure drag engendered by the separation of the flow away from the sphere near its equator. At a Reynolds number of about 3×10^5 for a smooth sphere the boundary layer undergoes transition to a turbulent state and the separation point moves aft over the downstream surface of the sphere, substantially reducing the pressure drag and hence the total drag. Values of C_D from 0.1 to 0.2 are obtained at Reynolds numbers greater than about 5×10^5 . Compressibility effects on the drag coefficient are large and nonlinear throughout the Reynolds number range of interest. The influence of transition to a turbulent boundary

^aReynolds number is the ratio of inertial to viscous forces: $Re = \rho Va/\mu$, where ρ = atmospheric density, V = fragment velocity relative to the atmosphere, a = fragment diameter and μ = dynamic viscosity. Drag coefficient is the ratio of the drag force to the product of the dynamic pressure and the fragment cross-sectional area, $C_D = D/(1/2 \rho v^2)(\pi a^2/4)$.

layer is evident only for Mach numbers^a below the critical value of about 0.5. At higher Mach numbers, the shock waves formed in the flow near the equator separate the boundary layer at this point for all Reynolds numbers of interest and no drag reduction occurs. For Mach numbers greater than 1.5, the drag coefficient is approximately 1.0, independent of Reynolds number.

The aforementioned discussion applied to smooth spheres and spheres roughened to about 3 percent of the diameter (about the roughness of a golf ball). The ejecta fragments under consideration, in particular, the larger fragments, are not spherical and the values for smooth or slightly roughened spheres do not apply. Drag coefficients for bluff shapes such as short blunt cylinders, wedges and so forth, with lengths nearly equal to the diameter or width, range from about 0.8 to 1.2 for Reynolds numbers greater than 10^3 . Of even greater significance than the generally higher level for bluff shapes, as compared to smooth spheres, is the observation that no drag decrease occurs in the critical Reynolds number range for bodies with sharp edges or blunt aft faces. This is due to the "fixing" of the point of boundary-layer separation at the sharp corner of the body. These observations apply to data obtained for cubes tumbling in an uncontrolled manner (data summarized by Hoerner, Reference 10). A value of C_D of 0.75 was obtained in the incompressible range for cubes. The influence of compressibility on the drag coefficients for bluff shapes and cubes is similar to that for smooth spheres, with C_D increasing to 1.2 for a Mach number of about 1.4, and remaining nearly constant at that value for higher Mach numbers.

Since ejecta fragments have been observed to be very rough and nonspherical in shape, the smooth sphere data were not incorporated into the ejecta model. The most important effect is the elimination of the drag decrease at the critical Reynolds number. The simplest approach employs an incompressible drag law of the form

^a Mach number is the ratio of the fragment velocity relative to the atmosphere to the speed of sound.

$$C_D = 0.6 + \frac{36}{Re} \quad (13)$$

The next step is to consider the effects of the air compressibility. A cross-plot of the data given by Hoerner (Reference 10), delineating the dependence of the smooth sphere drag coefficient on Mach number for Reynolds numbers of interest in the ejecta study, is shown in Figure 6. The range of drag coefficients given by Equation (13) for $10^3 < Re < 3 \times 10^5$ is from 0.60 to 0.64; thus, the incompressible drag coefficients are too low even for smooth spheres above a Mach number of about 0.7. Calculations are currently performed using a compressible drag law shown by the dashed lines in Figure 6. This compressible drag law has the following characteristics:

- It obeys Equation (13) for incompressible flow, defined here as $M \leq 0.4$ for all Reynolds numbers
- It fits data from Hoerner (Reference 10) for supersonic flow over bluff objects at high Reynolds numbers, defined here as $M \geq 1.2$ for $Re \geq 60$
- It obeys Equation (13) for slow viscous flow at all Mach numbers, defined here as $Re \leq 60$.

For the intermediate ranges of Reynolds and Mach numbers, the drag coefficient is determined by interpolating linearly between Equation (13) at $M = 0.4$ and $C_D = 1.2$ at $M = 1.2$. This procedure is shown in Figure 6 for two Reynolds numbers.

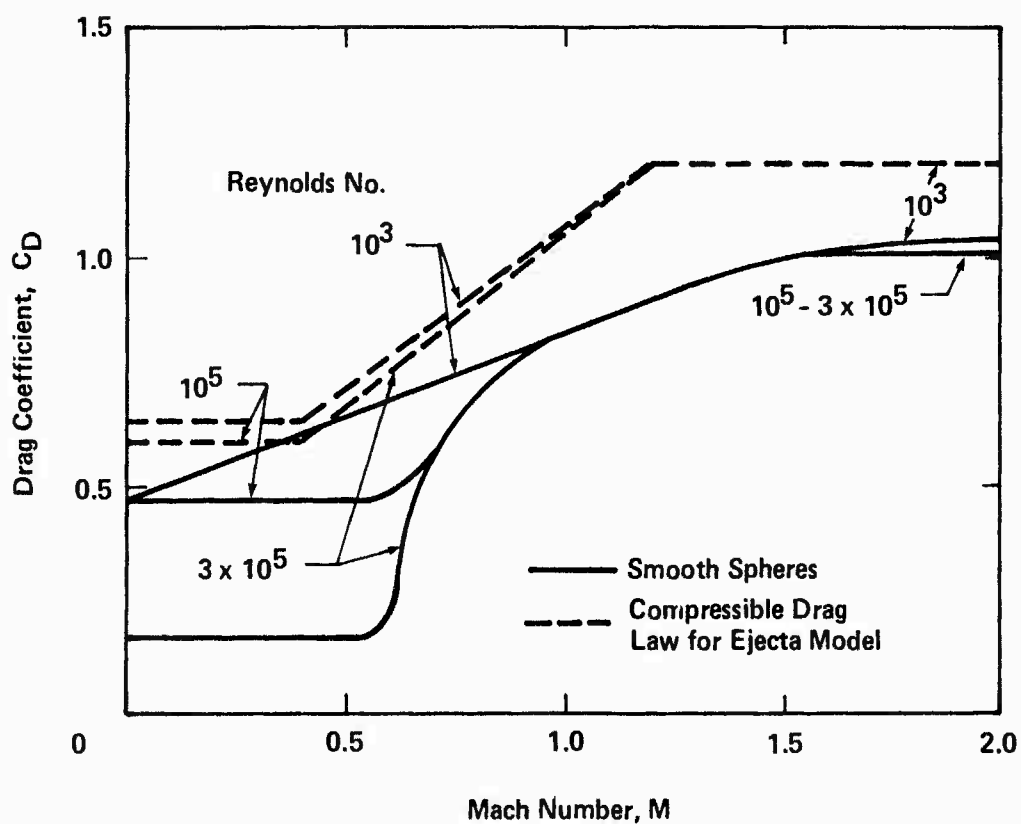


Figure 6. Fragment Drag Coefficients

Section 5

RESULTS AND DISCUSSION

Calculations of the ejecta deposition and cloud environments were performed for a 1 MT surface burst on hard rock. A matrix of 12,000 trace fragments was developed using Equations (1) and (7). The fragment diameter interval of 0.002 to 9 m was divided into 66 size classes of equal mass. The absolute maximum velocity was 566 m/sec [Equation (11)]. The size-dependent maximum velocity was obtained from Equation (12) using $C=0.1$.

The predicted ejecta depth is shown in Figure 7 (current model). The distribution begins at the apparent crater radius, 0.14 km. The peak depth of 3.2 m occurs at the crater lip radius, 0.17 km. The depth then decreases with increasing range out to the maximum range of 6.5 km. The initial decrease follows approximately an R^{-4} law. The depth between about 1 and 3 km range decreases by about $R^{-2.5}$. The distribution at larger ranges varies as R^{-5} . The R^{-3} law proposed by McGetchin et al. (Reference 2) for lunar craters is also shown in Figure 7. Finally, results obtained using the exponential model developed by Post (Reference 1) are given for the maximum (95 percentile), median (50 percentile) and minimum (5 percentile) ejecta thicknesses using a cratering efficiency of $0.84 \text{ m}^3/\text{ton}$ (equivalent to current model). Post's median correlation is within a factor of 2 of the results obtained using the current model out to a range of about 1.5 km. Beyond this range, the basic characteristics of the distributions are different (power law vs. exponential) and Post's median correlation drops below the results obtained using the current model. The exponential model thus appears to severely underpredict the ejecta depth at large ranges; however, the depth in this discontinuous ejecta regime is not a particularly significant parameter (see Figure 8, discussed below).

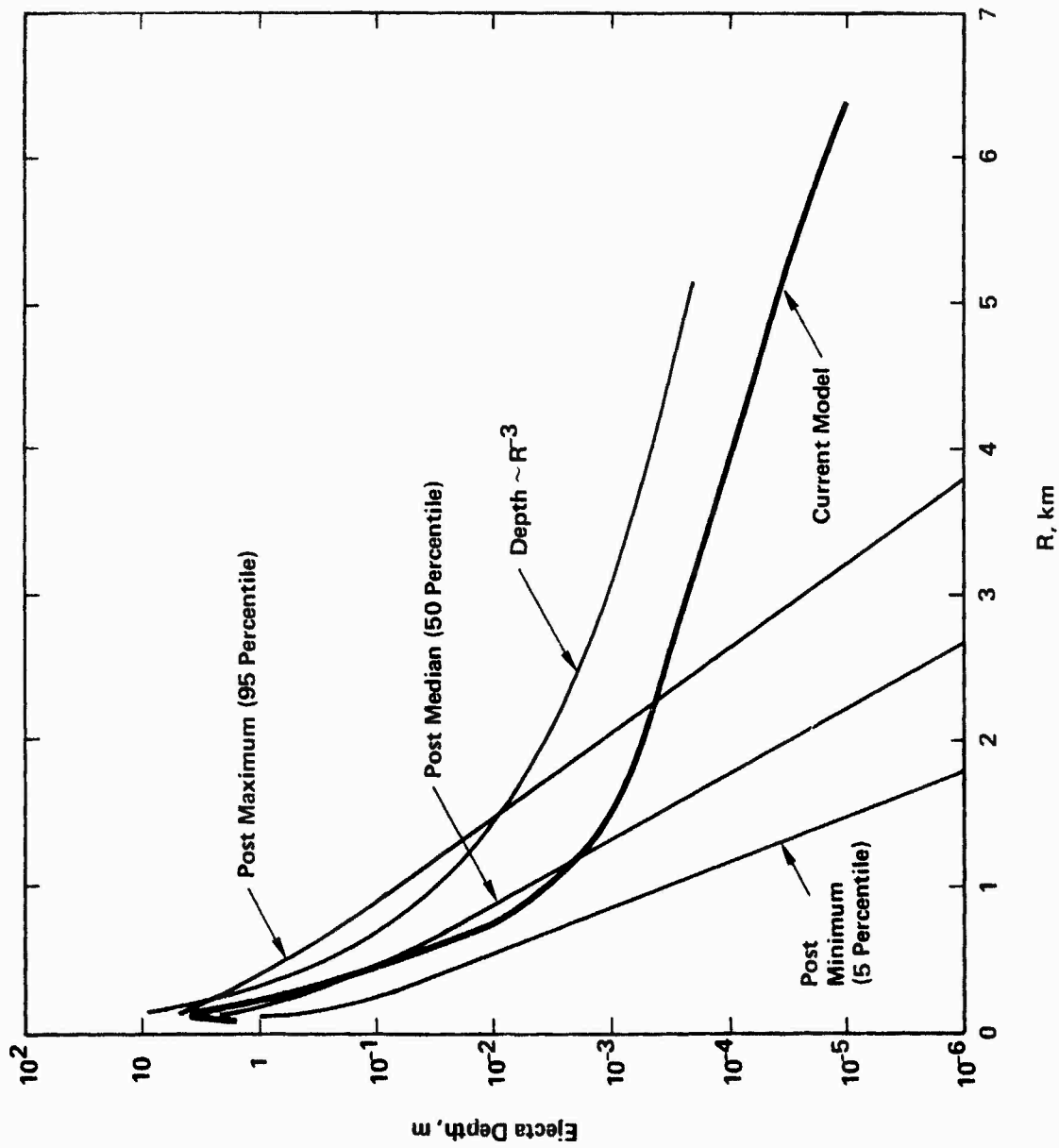


Figure 7. Ejecta Depth for 1 MT Surface Burst

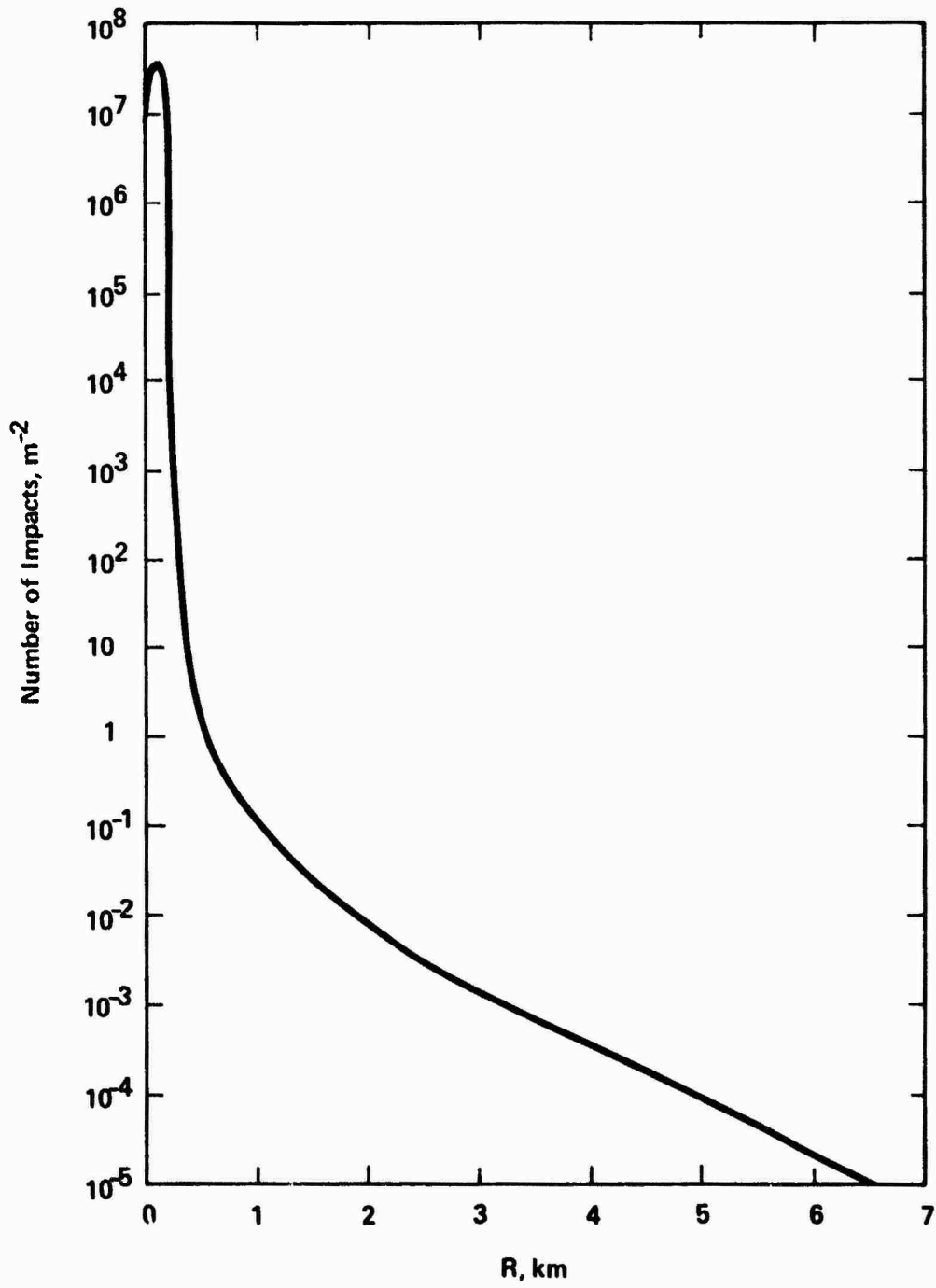


Figure 8. Ejecta Areal Number Density For 1 MT Surface Burst

The maximum (95 percentile) and minimum (5 percentile) curves of the Post model (Reference 1) account for the scatter in the experimental data base. This scatter is primarily a result of the azimuthal variations in the ejecta distribution pattern commonly known as rays. The current model does not have provisions for the determination of azimuthal effects. The uncertainty in the results introduced by model uncertainties other than azimuthal variations is estimated to be about a factor of 3 relative to the values shown in Figure 7. The estimation of 95 and 5 percentile limits for the current model, including ray effects, merits further research effort.

The ejecta areal mass density (mass deposited per m^2 surface area), which was presented in previous reports as the principal deposition parameter (see Reference 11, for example), may be obtained by multiplying the ejecta depths given in Figure 7 by the in situ density of the cratering medium. The corresponding areal number density (number of fragments deposited per m^2 surface area) is presented in Figure 8 for the 1 MT surface burst on hard rock. This parameter, which is not provided by the Post and McGetchin et al. models (References 1 and 2, respectively), exhibits a stronger range dependence than the depth distribution. The values below unity may be interpreted as impact probabilities (for example, there is a 10% probability of one impact per m^2 at a range of 1 km).

The primary reason for the high values of the areal number density in the crater lip region (Figure 8) is the preponderance of small fragments at the short ranges. The fragment size class (defined by the minimum and maximum size fragments reaching a given range) decreases with increasing range as indicated in Figure 9. This reduction is accompanied by a rapid reduction in the areal number density (Figure 8). The corresponding minimum and maximum values of the impact time, velocity and angle are shown in Figures 10, 11 and 12 respectively.

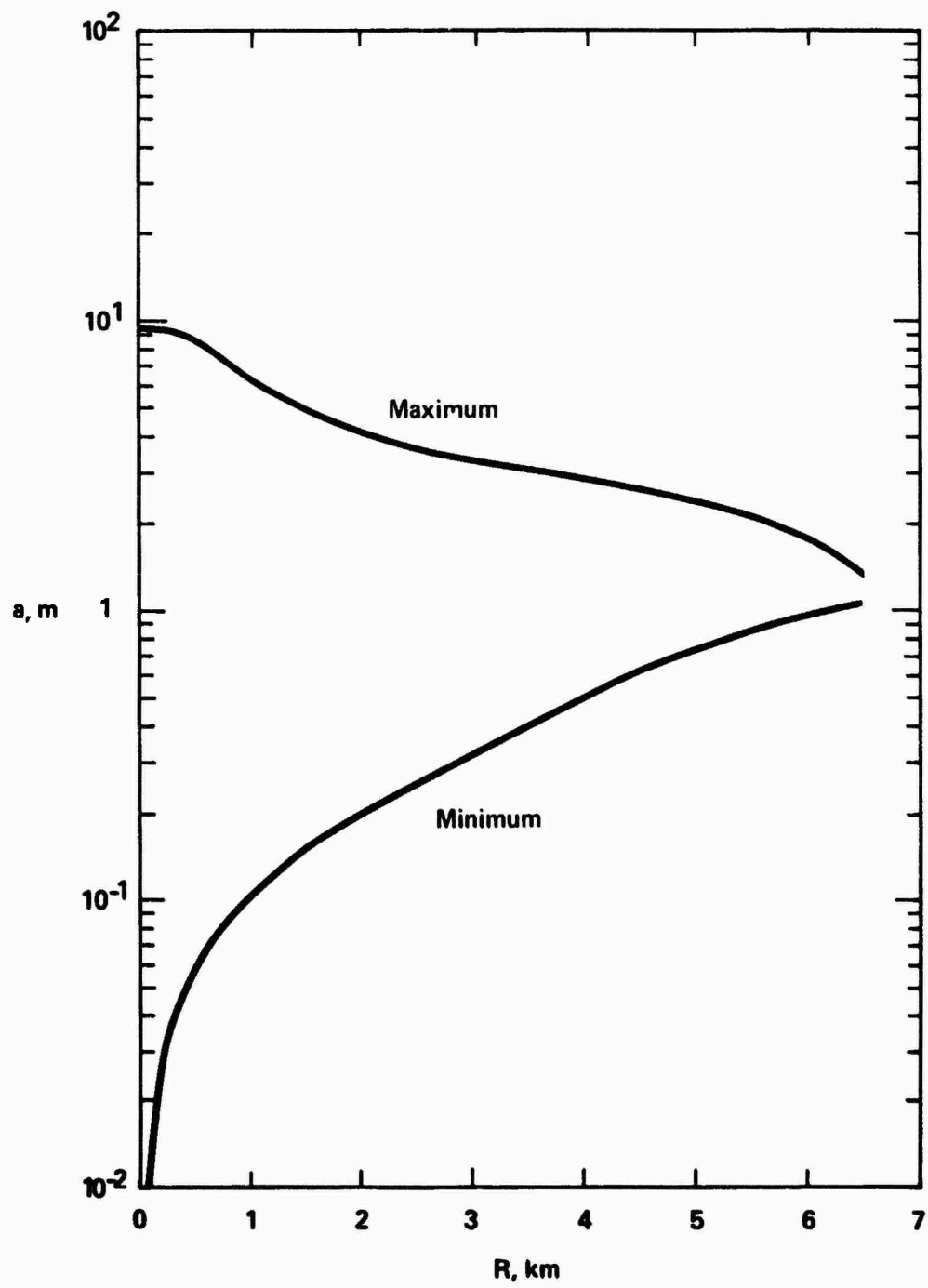


Figure 9. Ejecta Fragment Size Class for 1 MT Surface Burst

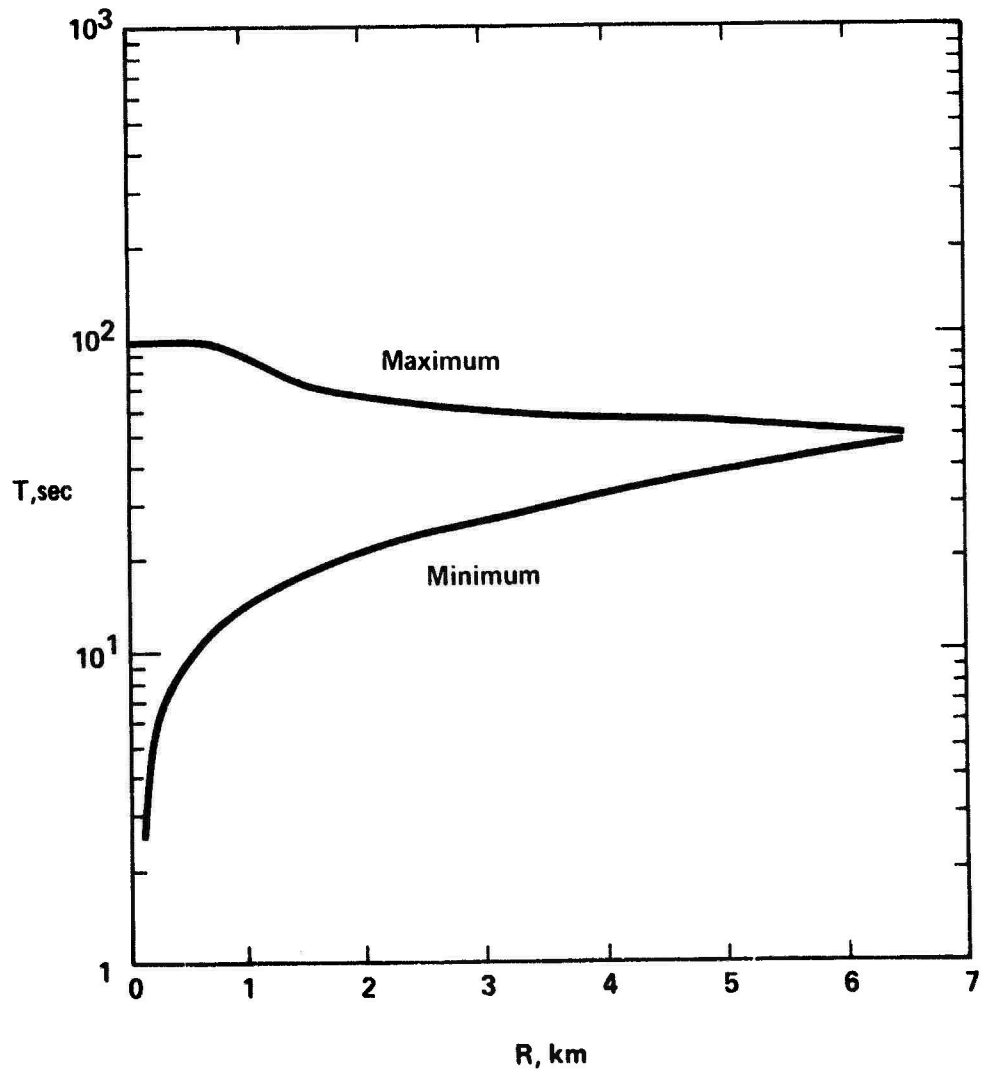


Figure 10. Ejecta Impact Time for 1 MT Surface Burst

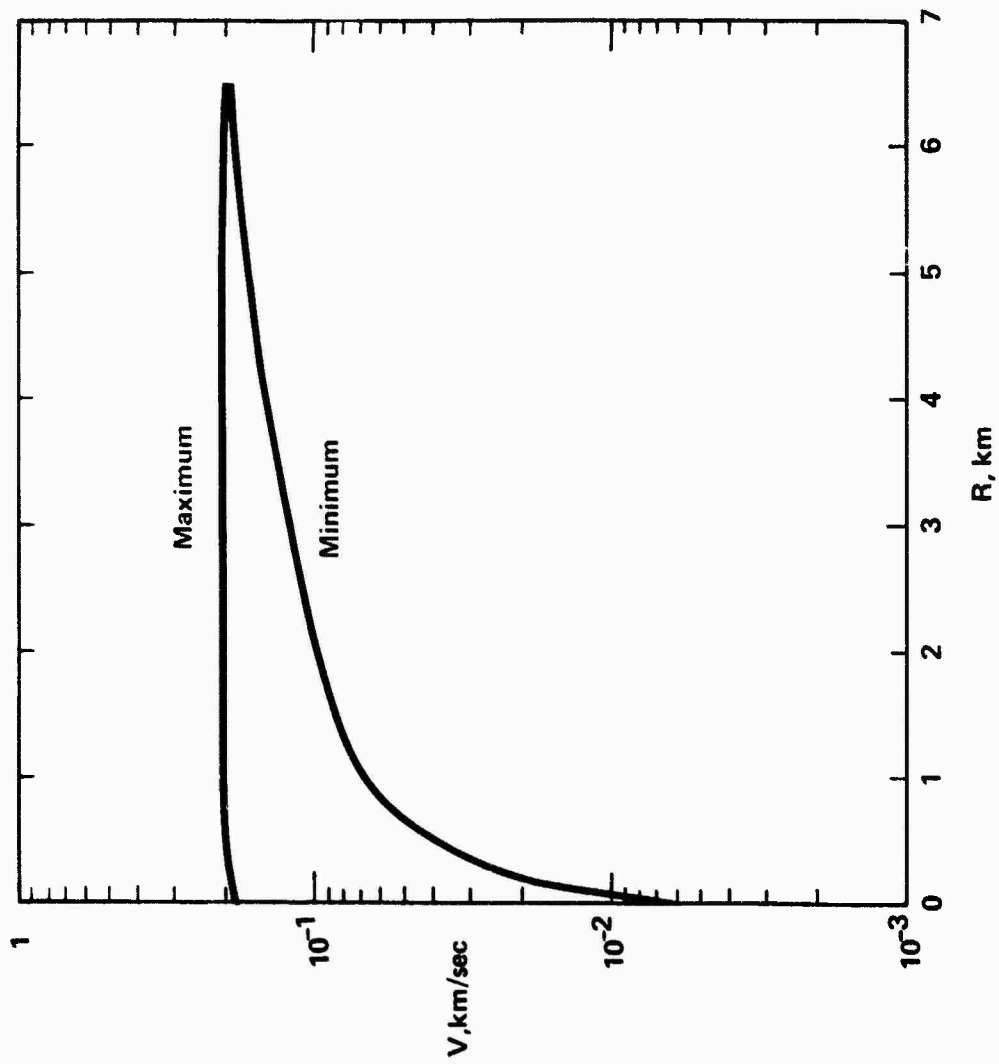


Figure 11. Ejecta Impact Velocity for 1 MT Surface Burst

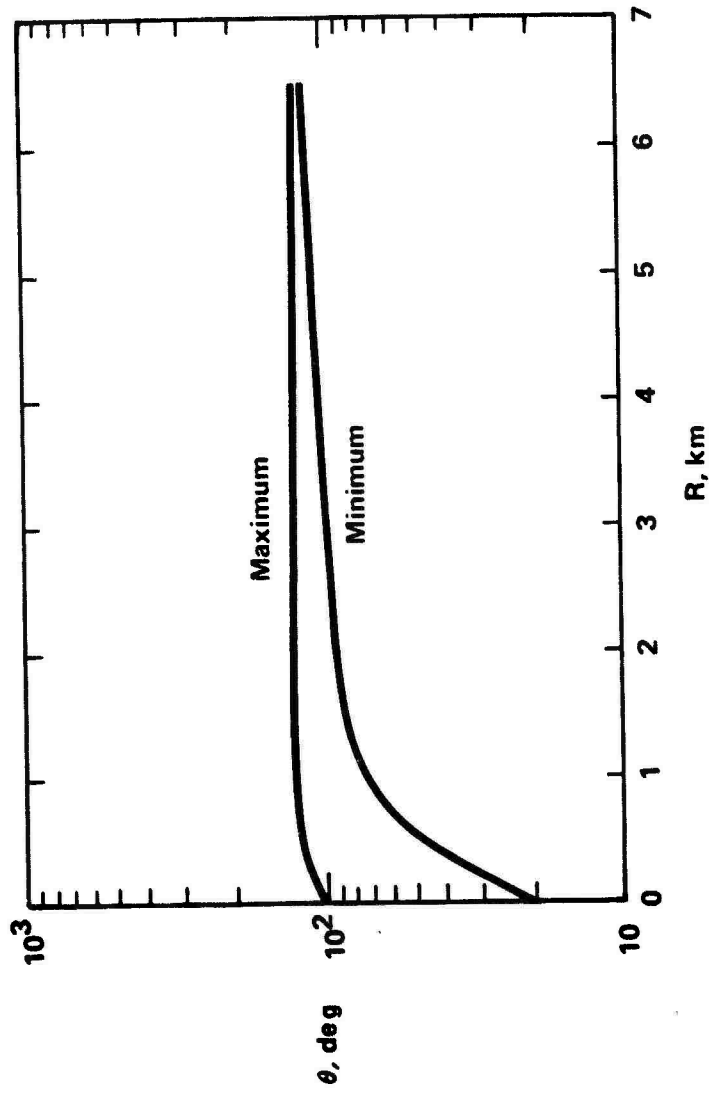


Figure 12. Ejecta Impact Angle for 1 MT Surface Burst

Ejecta cloud outlines for the 1 MT surface burst on hard rock are shown in Figure 13 for times from 5 through 50 seconds after burst. The ejecta is contained in a growing fan-shaped region (in two dimensions) at 5 seconds after burst. This region grows but maintains a similar shape to about 20 seconds after burst. After that time, the stem begins to form along the vertical axis as the smaller fragments are entrained by the rising fireball. The larger fragments fall toward the surface and away from the burst point. The ejecta cloud outline illustrates this behavior progressively from 30 to 50 seconds after burst. The entire outer region of ejecta fragments disappears by 55 seconds after burst, leaving the stem region in the center.

Density contours (number of fragments per m^3) may be constructed from the ejecta cloud description provided by the current model. Examples of these contours are shown in Reference 11.

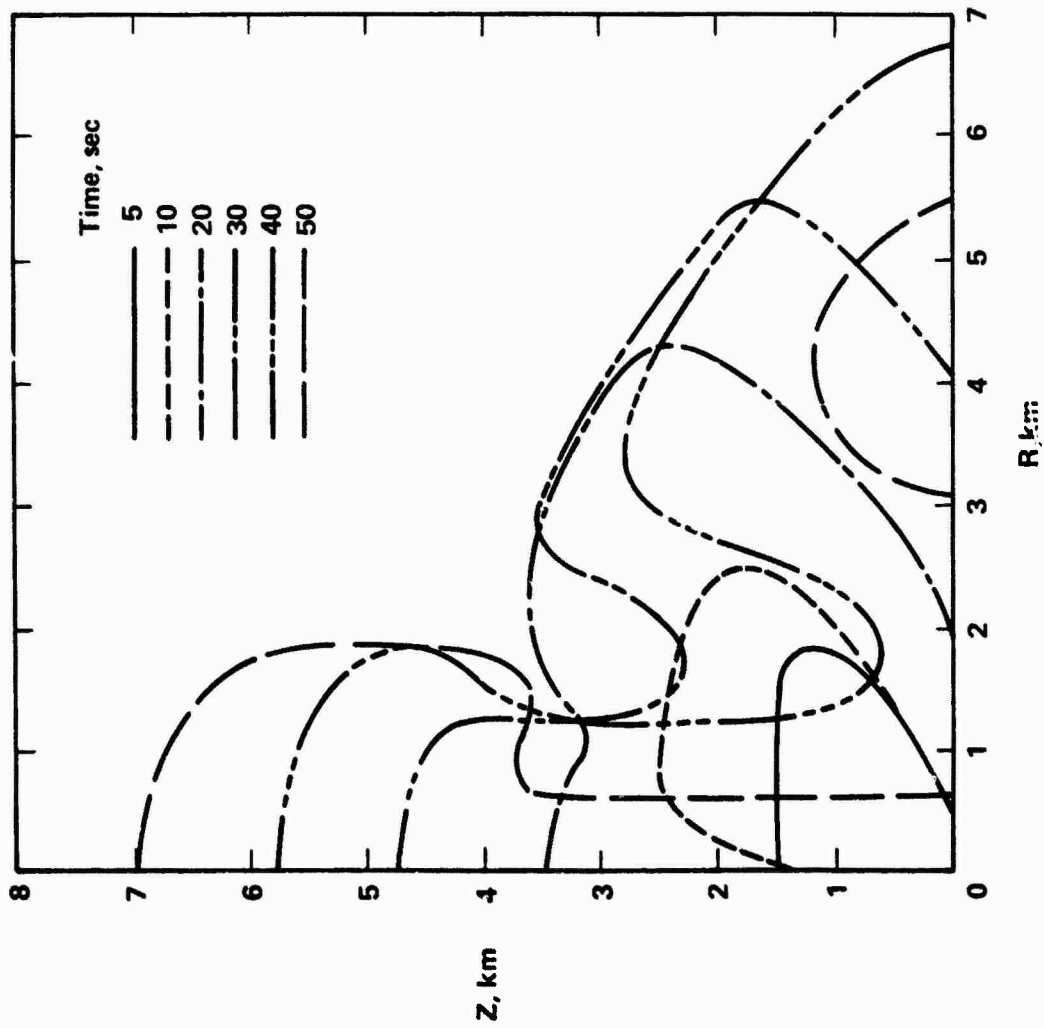


Figure 13. Ejecta Cloud Boundaries for 1 MT Surface Burst

Section 6

CONCLUDING REMARKS

A dynamic model for the high explosive and nuclear ejecta environments has been presented, together with selected results for a 1 MT nuclear surface burst on hard rock. The model provides both the ground deposition and airborne ejecta cloud environments. Predictions of the ejecta depth variation with range compare favorably with empirical correlations of other investigators.

The ejecta source model combines current theoretical and empirical results in a manner that permits calculations for general cases for which no data are available as well as for specific high explosive and nuclear events. The effects of explosive type, yield and geology are taken into account.

Two specific areas where further research would lead to significant advancements in the ejecta model have been identified. The first concerns the choice of source parameters for bursts in incohesive soils. The use of the in situ site distribution, including the maximum fragment size, will give substantially different results than if the correlations for cohesive soils are employed. This question requires further analysis of test data obtained from shots over dry incohesive soils for its satisfactory resolution. The second area of concern is that of ejecta rays. The scatter of nearly four orders of magnitude exhibited by models based on correlations of measured ejecta blanket thicknesses includes azimuthal variations. The current ejecta model, with an estimated uncertainty band of less than an order of magnitude, does not address the ray problem. Further research is required to determine the effects of rays on this uncertainty level.

REFERENCES

1. Post, R.L., Jr., "Ejecta Distributions from Near-Surface Nuclear and HE Bursts," Air Force Weapons Laboratory, TR-74-51, May 1974.
2. McGetchin, T.R., Settle, M. and Head, J.W., "Radial Thickness Variation in Impact Crater Ejecta: Implications for Lunar Basin Deposits," Earth Planet. Sci. Lett. 20, 1973.
3. Layson, W., Private Communication, General Research Corporation, August 1969.
4. Davis, L.K., and Carnes, B.L., "Operation Mine Shaft: Cratering Effects of a 100-Ton TNT Detonation on Granite," MS-2151, U.S. Army Engineer Waterways Experiment Station, February 1972.
5. Liner, R.T., Jr., Private Communication, Science Applications, Inc., June 1976.
6. Gault, D.E., Shoemaker, E.M. and Moore, H.T., "Spray Ejected from the Lunar Surface by Meteoroid Impact," NASA TND-1767, April 1963.
7. Wisotski, J., "Dynamic Ejecta Parameters from High Explosive Detonations," Paper Presented at Symposium on Planetary Cratering Mechanics, Flagstaff, Arizona, September 1976.
8. Sauer, F.M., and Cooper, H.F., "Crater-Related Ground Motions and Implications for Crater Scaling," Paper Presented at Symposium on Planetary Cratering Mechanics, Flagstaff, Arizona, September 1976.
9. Rosenblatt, M., and Eggum, G.E., Private Communication, California Research and Technology, May 1975.
10. Hoerner, S.F., Fluid-Dynamic Drag, Published by Author, 1965.
11. Seebaugh, W.R., "Studies of the Nuclear Crater Ejecta Environment," Science Applications, Inc., SAI-75-507-WA, DNA 3640F, June 1975.

NOMENCLATURE

Symbols

a	Fragment diameter; term in Equation (6)
C	Coefficient in Equation (12)
C_D	Drag coefficient
K_g	Geology correction factor
K_s	Source correction factor
m	Mass of fragment
M	Mass; Mach number
R	Range; radius
Re	Reynolds number
SHOB	Scaled height of burst
T	Time
V	Velocity
W	Yield
Z	Altitude
θ	Angle
μ	Dynamic viscosity
ρ	Material density

Subscripts

a	Apparent crater
al	Apparent crater lip
e	Ejecta
m, max	Maximum
min	Minimum
z	Vertical

DISTRIBUTION LIST

DEPARTMENT OF DEFENSE

Director
Defense Advanced Rsch. Proj. Agency
ATTN: NMRO
ATTN: PMO
ATTN: STO
ATTN: Technical Library

Director
Defense Civil Preparedness Agency
ATTN: Admin. Off.

Defense Documentation Center
12 Cy ATTN: TC

Director
Defense Intelligence Agency
ATTN: DT-1C
ATTN: DI-7E
ATTN: DB-4C, Edward O'Farrell

Director
Defense Nuclear Agency
ATTN: DDST
ATTN: STSI, Archives
2 Cy ATTN: SPSS
3 Cy ATTN: STTL, Technical Library

Dir. of Defense Rsch. & Engineering
ATTN: DD/TWP
ATTN: AD/SW
ATTN: S&SS(OS)

Commander
FC, DNA
ATTN: FCPR

Director
Interservice Nuclear Weapons School
ATTN: Document Control

Director
Joint Strat. Tgt. Planning Staff, JCS
ATTN: STINFO Library

Chief
Livermore Division, FC, DNA
ATTN: FCPRL

WWMCCS Systems Engineering Org.
ATTN: Thomas Neighbors

DEPARTMENT OF THE ARMY

Director
BMD Advanced Tech. Ctr.
ATTN: 1CRDABH-X
ATTN: CRDABH-S

Dep. Chief of Staff for Rsch. Dev. & Acq.
ATTN: Technical Library

Chief of Engineers
ATTN: DAEN-RDM
ATTN: DAEN-MCE-D

DEPARTMENT OF THE ARMY (Continued)

Deputy Chief of Staff for Ops. & Plans
ATTN: Technical Library

Commander
Harry Diamond Laboratories
ATTN: DRXDO-NP
ATTN: DRXDO-TI, Technical Library

Commander
Redstone Scientific Information Ctr.
ATTN: Chief, Documents

Director
U.S. Army Ballistic Research Labs.
ATTN: W. Taylor
ATTN: Technical Library, Edward Baicy
ATTN: J. H. Keefer, DRXBR-TL-IR
ATTN: Julius J. Meszaros, DRXBR-X

Commander
U.S. Army Engineer Center
ATTN: ATSEN-SY-L

Division Engineer
U.S. Army Engineer Div., Huntsville
ATTN: HNDED-SR

Division Engineer
U.S. Army Engineer Div., Ohio River
ATTN: Technical Library

Director
U.S. Army Engr. Waterways Exper. Sta.
ATTN: Technical Library
ATTN: Guy Jackson
ATTN: John N. Strange
ATTN: Leo Ingram
ATTN: William Flathau

Commander
U.S. Army Mat. and Mechanics Research Center
ATTN: Technical Library

Commander
U.S. Army Materiel Dev. and Readiness Command
ATTN: Technical Library

Commander
U.S. Army Nuclear Agency
ATTN: Technical Library

DEPARTMENT OF THE NAVY

Chief of Naval Research
Navy Department
ATTN: Code 464, Jacob L. Warner
ATTN: Nicholas Perrone
ATTN: Code 464, Thomas P. Quinn
ATTN: Technical Library

Officer-in-Charge
Civil Engineering Laboratory
Naval Construction Battalion Center
ATTN: Stan Takahashi
ATTN: Technical Library

DEPARTMENT OF THE NAVY (Continued)

Commander
David W. Taylor Naval Ship R. and O. Center
ATTN: Code L42-3, Library

Commander
Naval Facilities Engineering Command
ATTN: Code 04B
ATTN: Code 03A
ATTN: Technical Library

Director
Naval Research Laboratory
ATTN: Code 2600, Technical Library

Commander
Naval Surface Weapons Center
ATTN: Code WA501, Navy Nuc. Programs Office

Commander
Naval Surface Weapons Center
ATTN: Technical Library

President
Naval War College
ATTN: Technical Library

Commanding Officer
Naval Weapons Evaluation Facility
ATTN: Technical Library

Director
Strategic Systems Project Office
Navy Department
ATTN: NSP-43, Technical Library

DEPARTMENT OF THE AIR FORCE

A.F. Geophysics Laboratory, AFSC
ATTN: SUOL, AFCRL Research Library

A.F. Institute of Technology, AU
ATTN: Library, AFIT, Bldg. 640, Area B

A.F. Weapons Laboratory, AFSC
ATTN: DYT
ATTN: DEP, Jimmie L. Bratton
ATTN: DES-S, M. A. Plamondon
ATTN: OES-C, Robert Henny
ATTN: SUL

Headquarters
Air Force Systems Command
ATTN: Technical Library
ATTN: DLCAW

Commander
Foreign Technology Division, AFSC
ATTN: TD-BTA, Library

Headquarters, U.S.A.F./IN
ATTN: INATA

Headquarters, U.S.A.F./PR
ATTN: PRE

Headquarters, U.S.A.F./RD
ATTN: RDQSM

DEPARTMENT OF THE AIR FORCE (Continued)

Commander
Rome Air Development Center, AFSC
ATTN: EMTLD, Doc. Library

SAMSO/MN
ATTN: MMH

Commander in Chief
Strategic Air Command
ATTN: NRI-STINFO Library

ENERGY RESEARCH AND DEVELOPMENT ADMINISTRATION

University of California
Lawrence Livermore Laboratory
ATTN: Tech. Info., Dept. L-3

Los Alamos Scientific Laboratory
ATTN: Doc. Con. for G. R. Spillman
ATTN: Doc. Con. for R. J. Bridwell
ATTN: Doc. Con. for Reports Library

Sandia Laboratories
ATTN: Doc. Con. for Technical Library

Sandia Laboratories
ATTN: Doc. Con. for 3141, Sandia Rpt. Coll.

U.S. Energy Research & Development Administration
Albuquerque Operations Office
ATTN: Doc. Con. for Technical Library

U.S. Energy Research & Development Administration
Division of Headquarters Services
Library Branch, G-043
ATTN: Doc. Con. for Class. Tech. Library

U.S. Energy Research & Development Administration
Nevada Operations Office
ATTN: Doc. Con. for Technical Library

Union Carbide Corporation
Holifield National Laboratory
ATTN: Doc. Con. for Technical Library
ATTN: Civil Defense Research Project

OTHER GOVERNMENT AGENCIES

Department of the Interior
Bureau of Mines
ATTN: Technical Library

Department of the Interior
U.S. Geological Survey
ATTN: J. H. Healy
ATTN: Cecil B. Raleigh

DEPARTMENT OF DEFENSE CONTRACTORS

Aerospace Corporation
ATTN: Tech. Information Services

Agabian Associates
ATTN: M. Agabian

Applied Theory, Inc.
2 cy ATTN: John G. Trulio

DEPARTMENT OF DEFENSE CONTRACTORS (Continued)

Avco Research & Systems Group
ATTN: Research Library, A83D, Room 7201

Battelle Memorial Institute
ATTN: Technical Library

The BDM Corporation
ATTN: Technical Library

The Boeing Company
ATTN: R. M. Schmidt
ATTN: Aerospace Library

California Research & Technology, Inc.
ATTN: Ken Kreyenhagen
ATTN: Technical Library
ATTN: Sheldon Shuster

Calspan Corporation
ATTN: Technical Library

Civil/Nuclear Systems Corp.
ATTN: Robert Crawford

University of Dayton
Industrial Security Super. KL-505
ATTN: Hallock F. Swift

University of Denver
Colorado Seminary
ATTN: Security Officer for J. Wisotski

EG&G, Inc, Albuquerque Division
ATTN: Technical Library

Gard, Incorporated
ATTN: G. L. Neidhardt

General Electric Company
TEMPO-Center for Advanced Studies
ATTN: DASIAC

IIT Research Institute
ATTN: Technical Library

Institute for Defense Analyses
ATTN: IDA Librarian, Ruth S. Smith

Kaman Avidyne, Division of Kaman Sciences Corp.
ATTN: E. S. Criscione
ATTN: Technical Library

Kaman Sciences Corporation
ATTN: Library

Lockheed Missiles & Space Co., Inc.
ATTN: Technical Library

Lockheed Missiles & Space Co.
ATTN: Tech. Info. Center, D/Coll.
ATTN: Tom Geers, D/52-33, Bldg. 2D5

McDonnell Douglas Corporation
ATTN: Robert W. Halprin

Merritt Cases, Incorporation
ATTN: J. L. Merritt
ATTN: Technical Library

DEPARTMENT OF DEFENSE CONTRACTORS (Continued)

The Mitre Corporation
ATTN: Library

Nathan M. Newmark
Consulting Engineering Services
ATTN: Nathan M. Newmark

Physics International Company
ATTN: Doc. Con. for Robert Swift
ATTN: Doc. Con. for Tech. Lib.
ATTN: Doc. Con. for Dennis Orphal
ATTN: Doc. Con. for Charles Godfrey
ATTN: Doc. Con. for E. T. Moore
ATTN: Doc. Con. for Larry A. Behrmann
ATTN: Doc. Con. for Fred M. Sauer

R & D Associates
ATTN: Harold L. Brode
ATTN: Technical Library
ATTN: Jerry Carpenter
ATTN: Henry Cooper
ATTN: William B. Wright, Jr.
ATTN: Jerry Stockton
ATTN: Cyrus P. Knowles

Science Applications, Inc.
ATTN: D. E. Maxwell
ATTN: David Bernstein

Science Applications, Inc.
ATTN: Technical Library

Science Applications, Inc.
ATTN: William R. Seebaugh

Southwest Research Institute
ATTN: Wilfred E. Baker
ATTN: A. B. Wenzel

Stanford Research Institute
ATTN: George R. Abrahamson
ATTN: Burt R. Gasten

Systems, Science and Software, Inc.
ATTN: Technical Library
ATTN: Donald R. Grine
ATTN: Ted Cherry
ATTN: Thomas D. Riney

Terra Tek, Inc.
ATTN: Technical Library
ATTN: Sidney Green

Tetra Tech, Inc.
ATTN: Technical Library
ATTN: Li-San Hwang

TRW Systems Group
ATTN: Tech. Info. Center, S-193D
2 cy ATTN: Peter K. Dia, R1/217D
ATTN: I. E. Alber, R1-1008
ATTN: D. H. Baer, R1-2136
ATTN: R. K. Plebuch, R1-2D78

TRW Systems Group
ATTN: E. Y. Wong, 527/712

Universal Analytics, Inc.
ATTN: E. I. Field

DEPARTMENT OF DEFENSE CONTRACTORS (Continued)

URS Research Company
ATTN: Technical Library

The Eric H. Wang, Civil Engineering Research Facility
ATTN: Neal Baum
ATTN: Larry Bickle

Washington State University
Administrative Office
ATTN: Arthur Miles Hohorf for George Duval

DEPARTMENT OF DEFENSE CONTRACTORS (Continued)

Weidlinger Assoc., Consulting Engineers
ATTN: J. W. Wright
ATTN: Melvin L. Baron

Weidlinger Assoc., Consulting Engineers
ATTN: J. Isenberg

Westinghouse Electric Company
Marine Division
ATTN: W. A. Volz

